Pergamon

0301-9322(94)00090-5

Int. J. Multiphase Flow Vol. 21, No. 5, pp. 817–835, 1995

0301-9322/95 $9.50 + 0.00

CALCULATION OF THE DISCHARGE CHARACTERISTIC OF AN ORIFICE FOR GAS–LIQUID ANNULAR–MIST FLOW

R. FISCHER
MTU Motoren- und Turbinen-Union München GmbH, München, Germany

(Received 27 April 1993; in revised form 11 August 1994)

Abstract—A theoretical method for predicting the pressure drop discharge characteristic of low pressure two-component gas–liquid annular–mist flows through an orifice is presented. Its range of applicability includes incompressible, compressible and choked flow conditions. The flow model, upon which the method is based, takes into account the liquid separation in an annular liquid film flow and droplets in the gas core flow. For the resulting mist core flow, which determines the pressure drop behaviour across the orifice, an equivalent two-phase density is derived, which characterizes the compressibility of the mist fluid. The predictions of the present method are compared with predictions obtained by different methods known from the literature and with available experimental data for air–water and air–oil mixtures for different orifices and different inlet conditions. The agreement between the proposed method and measurements is good for subcritical as well as choked flow conditions.

Key Words: two-phase orifice flow, discharge characteristic, annular–mist flow, equivalent two-phase density, critical mass flow rate

1. INTRODUCTION

Two-phase flows through pipe systems are of great industrial interest. Besides well-known applications in the nuclear and chemical industries, two-phase flow is also an important topic in the development and design of modern aero-engines. An integral part of an aero-engine is the secondary air system, which is complex and affects the whole engine; this includes performance, economy, safety and reliability. One part of the secondary air system is the vent system, which has to vent an air–oil mixture, created in the bearing chambers by lubrication oil and sealing air through a pipe system from the bearing chambers to the air–oil separator. Besides the discharge capacity of the vent system, the pressure drop behaviour is an important item influencing the pressurization of the bearing chamber seals and as a result the safety and reliability of the engine. A malfunction can cause oil leakages leading to cabin air contamination or external oil fire. Therefore, the design of an advanced vent system requires suitable two-phase pressure drop models and correlations for different flow elements used in a vent pipe system; for example, bends, junctions and orifices (see Zimmermann *et al.* 1991). An important flow element is the vent restrictor (orifice), which is used to trim the vent system and which very often dominates the pressure drop characteristic of the system. Depending on the operating condition of the engine within the flight envelope, the two-phase flow through the orifice may be subcritical or choked and the mass flow quality of the air–oil mixture may vary significantly.

Consequently, there is a requirement for a simple but accurate method (design tool) for calculating the pressure drop of critical and subcritical two-component gas–liquid flows through orifices under aero-engine conditions. Because of the complexity of the secondary air system and its highly iterative calculation procedure (see Kutz & Speer 1992), CFD methods are not an appropriate design tool for practical engineering. Even for producing discharge characteristics for an orifice, depending on geometry, inlet condition and mass flow quality, CFD tools are too costly and time consuming.

In an attempt to obtain a quick and reliable tool, a method is described here which calculates the mass flow rate pressure drop characteristic (static pressures) for incompressible, compressible and choked gas–liquid flows through an orifice between the inlet and the throat (minimum area location). The pressure recovery by the succeeding sudden enlargement is neglected; this is a realistic assumption for practical applications. The applicability of the method is limited to

annular–mist flows at low pressures. The most important flow phenomena such as annular liquid film, liquid entrainment fraction and phase slip are considered, whereat the slip ratio is calculated without resort to an empirical slip-correlation. Consequently, the proposed method does not lend itself to a simple formula, but a set of equations which have to be solved numerically. However, the solution technique is much faster and significantly cheaper than more elaborate CFD methods.

The proposed method is compared with the well-known homogeneous equilibrium model, the method of Simpson (1983) for incompressible flows, the method of Morris (1991) for subcritical flows and the method of McNeil & Morris (1988) for critical flows. Furthermore, the proposed method is compared with experimental results from Chen *et al.* (1986) for air–water mixtures and with experimental results from Wood & Dickson (1973) for air–oil mixtures.

2. THEORY

The flow distribution of a gas–liquid two-phase flow through an orifice is highly complex and depends on geometrical boundary conditions, mass flow quality and the flow condition upstream of the restriction. In vent pipe systems of aero-engines, the vent restrictor normally represents a drastic reduction in the available flow cross-sectional area. Consequently, for subcritical as well as choked orifice flows, the flow condition upstream (and downstream) of the restrictor is distinctly subcritical. In numerous vent system tests with air–oil mixtures performed to investigate the pressure drop behaviour of individual flow elements as well as complete vent pipe systems, upstream of the orifice annular–mist flow has been identified as the prevailing flow pattern. This experimental evidence of a liquid film attached to the pipe wall (depending on mass flow quality, orifice geometry and the pressure ratio across the system), which is in agreement with flow pattern maps for pipe flows (e.g. Chisholm 1983) led to the proposed three-field separate flow model, which considers the basic phenomenon of liquid separation in an annular film flow and droplets in the gas core flow. This contrasts with other methods known from literature, in which a general separated flow model is usually adopted, independent of the prevailing flow pattern.

2.1. *Flow model and assumptions*

In order to develop a relatively simple approach, certain simplifications have to be made and the complex three-dimensional problem is reduced to a one-dimensional method. As shown in figure 1, upstream of the orifice, section 1, and at the throat of the orifice, section 3, a three-field separated flow pattern is assumed, consisting of a mist core flow and an annular liquid film flow attached to the wall. The assumed vena contracta effect, which is discussed below, is considered by a reduction of the geometrical orifice throat diameter d_{geo} to an effective orifice throat diameter d_{eff}. Section 2 is defined as the upstream limiting section for the liquid film flow around the orifice edge. The phenomenon of flow separation between sections 1 and 2 is not introduced in figure 1 but approximately considered in the later analysis. The gas–droplet mixture in the core is treated

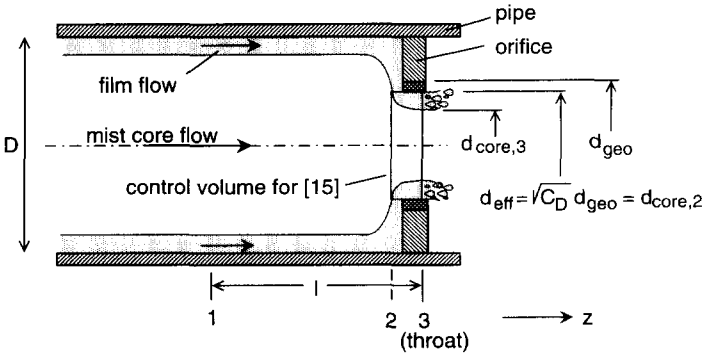

Figure 1. Flow model for annular–mist flow through a sharp edged orifice.

as a pseudo-fluid for which equivalent properties for velocity and density are defined. In contrast to other models, like for example the classic homogeneous equilibrium model or the model of Morris (1991), equivalent properties are defined for the core flow alone and not for the whole two-phase mixture. The liquid film is treated separated but coupled to the core flow. At section 1 the film thickness and film velocity can be described by empirical correlations. At the orifice throat, the proposed flow model of a liquid film represents a simplification of the real flow situation and may not be described by any simple correlations. However, independently from whether the "film liquid" in the orifice throat flows as film, as proposed, or as sheared-off droplets, the assumption can be made that a particle of fluid in the film just before entering the control volume between sections 2 and 3 has no velocity component in the z-direction.

The vena contracta effect, which is well-known for single fluid flows through orifices, is not well understood for two-phase flows. Recently some doubts have been raised by Morris (1990) whether a vena contracta exists at all for two-phase mixtures. By comparison of measured mass flow rates with mass flow rates calculated by the method of McNeil & Morris (1988), for choked gas–liquid flows through orifices, Morris found discharge coefficients close to unity. However, the obtained discharge coefficients correspond with the calculation method and are exclusively applicable to the method used and not of general validity. A method for estimating discharge coefficients for subcritical gas–liquid flows through orifices is proposed by Morris (1991). The discharge coefficients obtained are clearly below unity. The question whether a vena contracta occurs or not may heavily depend on the individual flow pattern. Starting with pure gas flow, the well-known vena contracta occurs. Decreasing the mass flow quality from unity, the droplet load in the gas flow increases from zero and may influence the contraction behaviour. Unfortunately, there is no clear evidence for the quantitative influence of different droplet loads on the vena contracta and for the question which minimum droplet load is required to obtain a significant influence on the discharge coefficient. In the proposed method, as a consequence of the proposed flow model, the mass flow quality in the mist core flow $\dot{x}_{\text{core}}$ is appreciably higher than the total mass flow quality. Depending on the diameter ratio of the orifice and the pressure ratio across the orifice, only a part of the total liquid flow rate is entrained in the core flow. For the remaining mist core flow the influence of the droplet load on the contraction is neglected and a vena contracta behaviour similar to that of pure gas flow is assumed. At least for low droplet loads this assumption represents a suitable approximation. In addition, it is assumed that the liquid film flow around the orifice edge does not significantly influence the vena contracta behavior of the core flow. Consequently, compressible discharge coefficients for single fluid air flows through orifices are applied to reduce the geometrical orifice diameter to the effective throat diameter used in the proposed flow model ($d_{\text{eff}} = C_{\text{D}}^{0.5} d_{\text{geo}}$). The basic incompressible discharge coefficient is obtained from Idel'chik (1986), the influence of the compressibility of the fluid on the discharge coefficient is taken into account by applying the well-known method of Bragg (1960).

As the model is one-dimensional, the distributions of gas velocity, droplet velocity and film velocity are assumed to be constant across the respective flow cross-section. Furthermore, the droplets in the gas core flow are assumed to be all of the same diameter and homogeneously distributed. The mass flow quality of the mist core flow is assumed to remain constant as the flow passes the orifice section, i.e. no droplet exchange between film and mist flow and no mass transfer is considered. The droplet acceleration in the contraction section is taken into account by applying a force balance on a spherical droplet and a simple approximation for the distribution of the gas velocity between the inlet and the throat cross section. From these assumptions and the resulting flow model, a complete set of equations can be obtained describing the annular–mist two-phase flow through an orifice.

2.2. Basic equations

For the annular–mist flow through an orifice, the total mass flow rate may be calculated by the following basic equation, which includes the effects of orifice geometry, fluid properties, inlet conditions at section 1 and the pressure ratio across the orifice:

$$\dot{M}_{\text{total}} = \dot{M}_{\text{core}} + \dot{M}_{\text{film}} = A_{\text{core}}[\epsilon \rho_{\text{G}} u_{\text{G}} + (1 - \epsilon)\rho_{\text{L}} u_{\text{drop}}] + A_{\text{film}} \rho_{\text{L}} u_{\text{film}}, \quad [1]$$

where ρ is the fluid density, u is the fluid velocity in the z-direction and A_{core} and A_{film} are the flow cross-sections of the core flow and the liquid film flow, respectively. The void fraction, which in [1] is applied to the core flow, is defined as:

$$\epsilon = \frac{\dot{x}_{core}\rho_L}{s(1-\dot{x}_{core})\rho_G + \dot{x}_{core}\rho_L}, \quad [2]$$

where $\dot{x}_{core}$ is the core mass flow quality and s is the phase slip ratio. In general, [1] may be applied to either the orifice inlet or the throat section. The unknown terms in [1] are determined by a set of equations, which describe the flow field between the inlet and the throat section. The most important equations are introduced below.

The well-known equations of conservation for mass, momentum and energy are valid for single fluid flows and equally for two-phase fluids. The steady-state one-dimensional continuity equation may be written in integral form as:

$$\int_A \rho u \, dA = 0, \quad [3]$$

and may be applied to the mist core flow as well as to the film flow.

Considering the mist core flow first, the gas–droplet mixture may be treated as a pseudo-fluid, which represents the two-phase fluid in its essential attributes and for which equivalent properties have to be defined. Introducing an equivalent density ρ_{eq}, which is considered in more detail in section 2.4, and introducing an equivalent velocity u_{eq}, which is defined below, the energy equation in differential form may be written for a pseudo-fluid as:

$$u_{eq}\, du_{eq} + \frac{1}{\rho_{eq}} dp = dr_\tau, \quad [4]$$

where the normal stress is neglected and r_τ is the specific friction term resulting from shear stress. For the equivalent two-phase velocity u_{eq}, which represents the transport velocity of mass, momentum and energy of a two-phase flow, a suitable definition has to be found. Based on a simple flow model with application to subcritical and choked flow conditions, Nguyen (1981) derived the following equation for the effective flow velocity of homogeneously distributed two-phase slip flows:

$$u_{eq} = \frac{u_G u_{drop}}{(1-\epsilon)u_G + \epsilon u_{drop}}. \quad [5]$$

Furthermore, for critical flow conditions Nguyen found the effective flow velocity u_{eq} to be identical with the velocity of sound a_{hom}, for which he derived the relationship introduced below. Although Nguyen verified this definition ([5]) only for critical flow conditions by comparison with experimental data obtaining excellent agreement, [5] is also assumed to be applicable to subcritical flow conditions. Possible inaccuracies due to the simple flow model might be maximum for the critical flow condition where the phase slip is maximum. The admissibility of this assumption is confirmed later by good results obtained by the proposed method. Consequently, [5] is proposed for substitution in [4], which may be applied to the mist core of the flow model and integrated between the inlet (section 1) and the throat (section 3) to yield the equation:

$$\tfrac{1}{2}(u_{eq,3}^3 - u_{eq,1}^2) - \int_1^3 \frac{1}{\rho_{eq}} dp - \frac{(\dot{E}_{film,3} - \dot{E}_{film,1})}{\dot{M}_{core}} = 0, \quad [6]$$

where p is the pressure and $\dot{E}_{film}$ is the kinetic energy flow rate of the annular liquid film, which receives its energy solely from the core flow. The equivalent density ρ_{eq}, which will depend on the gas density ρ_G, still has to be defined. In order to calculate the integral in [6], the gas density in the core flow between sections 1 and 3 has to be described. This can be easily done by the polytropic equation:

$$\frac{p}{p_1} = \left(\frac{T}{T_1}\right)^{n/(n-1)} = \left(\frac{\rho}{\rho_1}\right)^n, \quad [7]$$

where T is the fluid temperature and n is the polytropic coefficient, which may be calculated as follows. By considering the complete flow field, i.e. film flow and core flow, where now the gas–droplet mixture in the core is not treated as a pseudo-fluid, the energy conservation equation may be written as:

$$\sum E_{\mathrm{kin},i} + \sum H_i = \text{constant}, \quad i = \mathrm{G, drop, film} \tag{8}$$

where E_{kin} is the kinetic energy and H the enthalpy of the gas, droplet and film flows, respectively. Assuming an adiabatic two-phase flow, the total energies in sections 1 and 3 are equal and [8] may be rewritten as:

$$\sum \frac{1}{2} \dot{M}_i (u_{i,3}^2 - u_{i,1}^2) + \sum \dot{M}_i c_{\mathrm{p}i} (T_3 - T_1) = 0, \quad i = \mathrm{G, drop, film}, \tag{9}$$

where c_{p} is the specific heat. By introducing the entrainment fraction EF, which is considered in more detail in section 2.3, the individual mass flow rate $\dot{M}_i$ for gas, droplet and film may be expressed by the total mass flow quality $\dot{x}$ and the core mass flow quality $\dot{x}_{\mathrm{core}}$, respectively. Furthermore, by using [7] the temperature ratio T_3/T_1 may be expressed by the pressure ratio p_3/p_1 and the polytropic coefficient n, and [9] may be resolved for the polytropic coefficient. After some algebra the final equation for the polytropic coefficient reads as

$$n = \left[1 - \frac{\ln R}{\ln\left(\dfrac{p_3}{p_1}\right)} \right]^{-1}, \tag{10}$$

with

$$R = \frac{1 + \dfrac{(1-\dot{x}_{\mathrm{core}})}{\dot{x}_{\mathrm{core}}} \dfrac{c_{\mathrm{pL}}}{c_{\mathrm{pG}}} - \dfrac{u_{\mathrm{G},3}^2 - u_{\mathrm{G},1}^2}{2 c_{\mathrm{pG}} T_1} - \dfrac{(1-\dot{x}_{\mathrm{core}})}{\dot{x}_{\mathrm{core}}} \dfrac{u_{\mathrm{drop},3}^2 - u_{\mathrm{drop},1}^2}{2 c_{\mathrm{pG}} T_1} - (1-\mathrm{EF}) \dfrac{(1-\dot{x})}{\dot{x}} \dfrac{u_{\mathrm{film},3}^2 - u_{\mathrm{film},1}^2}{2 c_{\mathrm{pG}} T_1}}{1 + \dfrac{(1-\dot{x}_{\mathrm{core}})}{\dot{x}_{\mathrm{core}}} \dfrac{c_{\mathrm{pL}}}{c_{\mathrm{pG}}}} \tag{11}$$

In order to describe the flow condition of the core flow in the orifice throat, the interaction between gas and droplet flow during the contraction passage resulting in a droplet acceleration and a momentum and energy loss for the gaseous phase has to be considered and taken into account. Usually this is done by the introduction of a method for calculating the slip ratio s, either by empirical correlations or by theoretically derived equations (see, for example, Chisholm 1983). Whilst for two-phase pipe flows (subcritical and critical) several promising slip correlations exist, especially for two-phase orifice flows there is a lack of suitable correlations in the literature.

Therefore, in the proposed method, the droplet acceleration in the contraction passage and consequently phase slip and void fraction in the orifice throat are calculated by a simple force balance model applied to the droplets. This allows at least an approximate consideration of orifice geometry and pressure ratio across the orifice. Assuming spherical droplets, the droplet acceleration may be described by:

$$u_{\mathrm{drop}}(z) \frac{\mathrm{d}u_{\mathrm{drop}}}{\mathrm{d}z} = \frac{6}{8} c_{\mathrm{drag}} \frac{1}{h} \frac{\rho_{\mathrm{G}}}{\rho_{\mathrm{L}}} [u_{\mathrm{G}}(z) - u_{\mathrm{drop}}(z)]^2, \tag{12}$$

where h is the droplet diameter and c_{drag} is the drag coefficient. The droplet diameter has been found to be of minor influence on the calculated total mass flow rate. Even for flows with low mass flow qualities (high droplet loads) a variation of the droplet diameter in the relevant range $h = 0.05$–0.5 mm causes maximum changes in the calculated total mass flow rate of only a few percent. Because of this weak diameter dependence the use of a constant droplet diameter appears to be justified (no additional iteration in the calculation procedure). Furthermore, it is possible to evade the principle uncertainties regarding the choice of the diameter definition, which is

appropriate for the problem considered here. In the proposed method, the volume mean diameter is assumed to be the relevant diameter definition and an averaged volume mean diameter of $h = 100\ \mu m$ is used, which is representative for the fluids and the pressure levels considered here. However for other, distinctly different pressure levels, like for example in vent systems at high flight altitudes, the dependency of the droplet diameter on the pressure should be considered. It is proposed to calculate the droplet diameter (volume mean diameter) by the correlation of Kataoka *et al.* (1983), which is derived for droplet generation in annular two-phase pipe flows and which has been found to correlate experimental data with reasonable accuracy. For the drag coefficient a constant value of $c_{drag} = 0.46$ is used, which is valid for Reynolds numbers in the range of about $1000 \leqslant Re \leqslant 10^5$ (see Prandtl *et al.* 1984 and Wallis 1969).

In order to integrate [12] additional boundary conditions are required. The contraction length between sections 1 and 3 is assumed to be similar to that of single-phase gas flows and may be approximated by:

$$l \approx 2d\left(1 - \left(\frac{d}{D}\right)^2\right), \qquad [13]$$

where here d is the orifice throat diameter and D the pipe diameter. Assuming a quadratic variation for the diameter of the gas flow cross-section between inlet and throat with respect to the phenomenon of flow separation, the cross-sectional area variation is of fourth order. Because the basic gas dynamic equation for the flow cross-section area (see the flow function defined by [A7]) may be approximated for subcritical flow conditions by a simple parabolic equation $[M^* \sim (A^*/A)^2]$, for subcritical flow conditions the flow velocity is approximately $u \sim 1/A^2$, and hence the gas velocity in the contraction passage may be approximated by:

$$u_G(z) \approx u_{G,1} + (u_{G,3} - u_{G,1})\left(\frac{z}{l}\right)^8. \qquad [14]$$

The phase slip at the inlet cross-section, where the flow condition in each case is subcritical, is estimated by the simple correlation $s_1 \approx 1 + d/D$. For pipe flows, a slip ratio of 2 is obtained, which is in acceptable agreement with experimental data (see Nguyen 1981). Altogether, several simplications and approximations are necessary to calculate the phase slip and consequently the void fraction in the orifice throat. Compared with commonly used phase slip correlations, the proposed procedure is appreciably more complicated. However, the proposed procedure allows the calculation of the phase slip under consideration of the "flow history" upstream of the orifice throat and consequently under consideration of the orifice geometry and the pressure ratio across the orifice.

Considering the film flow, the momentum equation may be applied to the control volume between sections 2 and 3, shown in figure 1. By neglecting wall friction and with the assumption that the liquid film enters the control volume without having a momentum in the z-direction, the momentum equation in combination with gas dynamic equations reduces, after some algebra, to an equation for $A_{core,3}$:

$$(A_{eff} - A_{core,3})^2 + \frac{C_1}{C_2}(A_{eff} - A_{core,3}) - \frac{C_3}{C_2} = 0, \qquad [15]$$

where C_1, C_2 and C_3 are functions of $u_{G,3}$, p_3, $\rho_{G,3}$, c_3, A_{eff} and $A_{core,3}$. The derivation of [15] and the associated functions C_1, C_2 and C_3 are given in appendix A.

2.3. Film thickness and entrainment rate

The flow pattern of annular–mist pipe flow has already been the subject of a considerable amount of experimental and theoretical work resulting in numerous correlations for calculating film thickness, entrainment rate and other relevant parameters. For this reason, no details are given here about the theory of annular–mist pipe flow; the interested reader is referred to Kulov *et al.* (1979), Ishii & Mishima (1989) and Azzopardi *et al.* (1991).

To calculate the mean film thickness in this work, the empirical correlation of Kulov *et al.* (1979) is used, which is based on air–water experiments carried out in a straight vertical perspex tube of 25 mm diameter and 2 m length. The correlation for the film thickness b is given as:

$$\frac{b}{\theta} = 62.6\,\mathrm{Re}_L^{0.52}\,\mathrm{Re}_G^{-0.61}, \qquad [16]$$

where the reduced film thickness is given as:

$$\theta = \left[\frac{\nu_L^2}{g}\right]^{1/3}, \qquad [17]$$

and ν is the kinematic viscosity and g the acceleration due to gravity. The Reynolds numbers Re_L and Re_G are defined with the liquid mass flux based on the pipe cross-section and the gas mass flux based on the core cross-section, respectively. As the dynamic viscosity of the liquid was varied by the authors from 10^{-3} to $2.5\ 10^{-2}$ Ns/m^2 by using water–glycerol mixtures, it is assumed that this correlation can also be applied to air–oil mixtures in aero-engines in which the oil viscosity is comparable.

The entrainment fraction in cross-section 1, which is assumed to be constant for the whole orifice flow according to the flow model, is calculated by the empirical correlation of Ishii & Mishimi (1989). For low viscosity fluids, such as water or oil at higher temperatures, where the roll wave entrainment mechanism is the predominant mode of entrainment, these authors found for the fully developed entrainment fraction, EF, far away from the entrance region the correlation:

$$\mathrm{EF} = \frac{\dot{M}_{L,\mathrm{drops}}}{\dot{M}_{L,\mathrm{total}}} = \tanh[7.25\ 10^{-7}\,\mathrm{We}^{1.25}\,\mathrm{Re}_L^{0.25}], \qquad [18]$$

where the effective Weber number for entrainment is defined by

$$\mathrm{We} = \frac{\rho_G w_G^2 D}{\sigma}\left(\frac{\Delta\rho}{\rho_G}\right)^{1/3}, \qquad [19]$$

where w_G is the superficial gas velocity, D is the pipe diameter and σ the surface tension. Based on the entrainment fraction EF, the general definition for the mass flow quality $\dot{x}$ may be applied to the total two-phase flow, resulting in the total mass flow quality

$$\dot{x} = \frac{\dot{M}_G}{\dot{M}_G + \dot{M}_{L,\mathrm{total}}}, \qquad [20]$$

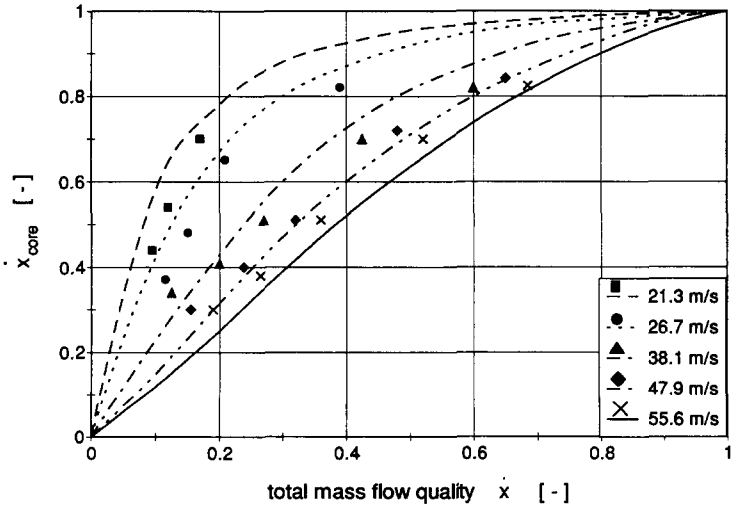

Figure 2. Core mass flow quality of an annular–mist pipe flow for air–water at $p_1 = 1.21$ bar and $T_1 = 298$ K (curves are present predictions, symbols are measurements of Andreussi *et al.*).

but also to the mist core flow of the annular–mist flow alone, resulting in the core mass flow quality

$$\dot{x}_{\text{core}} = \frac{\dot{M}_{\text{G}}}{\dot{M}_{\text{G}} + \dot{M}_{\text{L,drops}}} = \frac{1}{1 + \left(\frac{1-\dot{x}}{\dot{x}}\right) \text{EF}}. \quad [21]$$

In figure 2, the core mass flow quality $\dot{x}_{\text{core}}$ is plotted versus the total mass flow quality $\dot{x}$ for different gas velocities using [18] and [21] and compared with experimental data from Andreussi *et al.* (1978) for air–water mixtures. The agreement between calculation and measurement is reasonable. The distribution of the curves in figure 2 shows that the phenomenon of liquid separation in an annular film flow and droplets in the gas core flow must not be neglected.

2.4. Derivation of an equivalent two-phase density

According to the proposed flow model, the mist core flow determines the pressure drop across the orifice. Therefore, for the mist core flow, a suitable flow model has to be derived which describes the gas–droplet mixture in its essential attributes and especially its compressibility. This is realized by treating the gas–droplet mixture as a pseudo-fluid for which a suitable equivalent density has to be defined. The well-known definitions for two-phase densities such as the homogeneous density, the momentum density and others are all based on general separated flow models, which do not take into account the effects of individual flow patterns. Furthermore, these definitions are not consistent with the effective flow velocity u_{eq} defined by [5] and are, therefore, less suitable for the application in [6]. A more suitable definition for the equivalent density may be derived by considering the speed of sound, which characterizes the compressibility of a fluid.

For single-phase fluids the speed of sound may generally be expressed as:

$$a^2 = \frac{1}{\rho k}, \quad [22]$$

with the isotropic coefficient of volumetric expansion

$$k = -\frac{1}{V}\left(\frac{\partial V}{\partial p}\right)_{\text{is}}, \quad [23]$$

where V is the volume. Thus, it is possible to write

$$a_i^2 = \left(\frac{\mathrm{d}p}{\mathrm{d}\rho_i}\right)_{\text{is}}, \quad \text{where } i = \text{L, G}. \quad [24]$$

The fact that [24] is valid for gases as well as liquids suggests the assumption that the sonic velocity of a homogeneously distributed gas–liquid mixture can be expressed by an equivalent equation. Consequently, the sonic velocity of a homogeneously distributed two-phase mixture is defined by

$$a_{\text{eq}}^2 = \left(\frac{\mathrm{d}p}{\mathrm{d}\rho_{\text{eq}}}\right)_{\text{is}}, \quad [25]$$

where ρ_{eq} is an equivalent two-phase density, which may be derived from [25] in combination with a relationship for a_{eq}. In the literature several models and methods exist for calculating the velocity of sound in two-phase mixtures; a short survey is given for instance by Nguyen. In order to obtain for critical flow conditions consistency between the pressure drop ($\mathrm{d}v_{\text{eq}}\dot{m}^2 = \mathrm{d}p$, whereat Nguyen found for choked flows $u_{\text{eq}} = a_{\text{hom}}$) and the momentum flux ($a_{\text{eq}}^2 = \mathrm{d}p/\mathrm{d}\rho_{\text{eq}}$), the relationship of Nguyen has to be used for calculating the sonic velocity of a homogeneously distributed gas–liquid mixture:

$$a_{\text{hom}} = \frac{1}{(1-\epsilon)\sqrt{\frac{(1-\epsilon)}{a_{\text{L}}^2} + \frac{\rho_{\text{L}}}{\rho_{\text{G}}}\frac{\epsilon}{a_{\text{G}}^2}} + \epsilon\sqrt{\frac{\epsilon}{a_{\text{G}}^2} + \frac{\rho_{\text{G}}}{\rho_{\text{L}}}\frac{(1-\epsilon)}{a_{\text{L}}^2}}}, \quad [26]$$

where a_{L} and a_{G} are the single fluid sonic velocities for the liquid phase and the gaseous phase, respectively. In Nguyen's model, the interface of one phase is acting as the elastic wall of the other

phase and vice versa. A typical distribution for the two-phase sonic velocity is shown in figure 3, where a_{hom} is plotted against the void fraction ϵ for an air–water mixture for two different pressures. An increase in pressure, although not greatly affecting the trend, does significantly increase the value of a_{hom}. The comparison of [26] with experimental data from Semenov *et al.* (1967) shows good agreement for void fractions below 0.6 but appreciable deviations for higher void fractions.

By equating a_{eq} from [25] with [26], one obtains after some algebra

$$\frac{d\rho_{eq}}{dp} = (1-\epsilon)A\frac{d\rho_L}{dp} + \epsilon B\frac{d\rho_G}{dp} \quad [27]$$

with

$$A = (1-\epsilon)^2 + 2\epsilon(1-\epsilon)\sqrt{\frac{\rho_G}{\rho_L}} + \epsilon^2\frac{\rho_G}{\rho_L} \quad [28]$$

$$B = (1-\epsilon)^2\frac{\rho_L}{\rho_G} + 2\epsilon(1-\epsilon)\sqrt{\frac{\rho_L}{\rho_G}} + \epsilon^2. \quad [29]$$

Because an exact solution of [27] in a mathematically closed form across the complete range of void fractions (interpreting it as a total differential equation) does not exist, the hypothesis is made that the equivalent density ρ_{eq} may be expressed in the form

$$\rho_{eq} = f_1(\epsilon, \rho_L) + f_2(\epsilon, \rho_G), \quad [30]$$

where f_1 and f_2 first are unknown functions. Deriving the total differential of [30] and neglecting the pressure dependence of the void fraction ϵ as a good approximation for gas–liquid flows with high mass flow qualities and $\rho_G \ll \rho_L$, one obtains:

$$\frac{d\rho_{eq}}{dp} \approx \frac{\partial f_1}{\partial \rho_L}\frac{d\rho_L}{dp} + \frac{\partial f_2}{\partial p_G}\frac{d\rho_G}{dp}, \quad [31]$$

where the differential quotients of the functions f_1 and f_2 may be determined by comparing [31] with [27]. Consequently, [31] may be integrated considering the void fraction as a constant and the associated integration functions and integration constants may be determined by using the boundary conditions for ρ_{eq}:

$$\rho_{eq} = \rho_i, \quad i = L, G \quad \text{for } \epsilon = 0, 1$$

$$\frac{\partial \rho_{eq}}{\partial \epsilon} = 0, \quad \text{for } \epsilon = 0, 1.$$

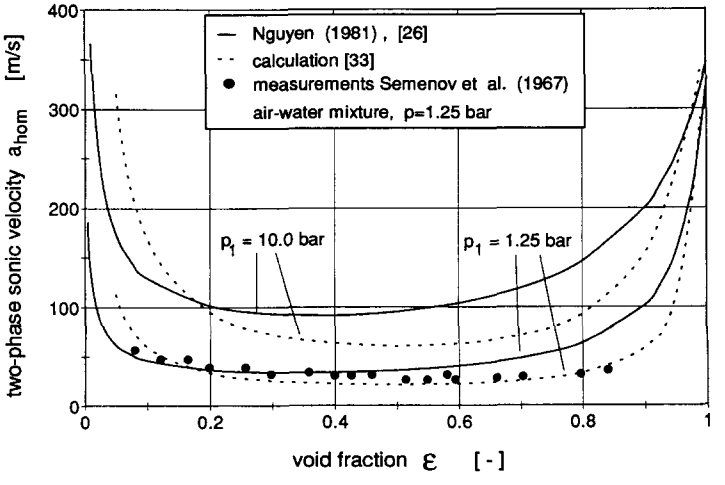

Figure 3. Two-phase sonic velocity for a homogeneous air–water mixture.

The resulting relationship for the equivalent density has the form

$$\rho_{eq} \approx (1-\epsilon)^3\rho_L + 3\epsilon(1-\epsilon)^2\rho_L + 3\epsilon^2(1-\epsilon)\rho_G + \epsilon^3\rho_G, \quad [32]$$

and is valid for homogeneously distributed gas–liquid flows, analogous to [26]. Because Nguyen verified [26] for subcritical flow conditions by comparison with experimental data, [32] is applicable to subcritical as well as critical flow conditions and may be used in [6]. In order to assess [32] and the simplification made by the neglect of the pressure dependence of the void fraction ϵ, the two-phase sonic velocity is recalculated by substituting [32] in [25]. The resulting equation

$$a = \left\{\left[4\epsilon^3(1-\epsilon) + 3(1-\epsilon)^2\epsilon^2\left(2\frac{\rho_L}{\rho_G} - 1\right) + \epsilon^4\right]\frac{1}{a_G^2} + \left[(1-\epsilon)^4 + 4(1-\epsilon)^3\epsilon + 3(1-\epsilon)^2\epsilon^2\left(2\frac{\rho_G}{\rho_L} - 1\right)\right]\frac{1}{a_L^2}\right\}^{-1/2} \quad [33]$$

is compared in figure 3 with results of [26] and with experimental data of Semenov *et al.* As can be seen, for both pressures p_1, the two calculation methods show the same trend in the two-phase sonic velocity. As expected, for the lower pressure $p_1 = 1.25$ bar the agreement between the two calculation methods is reasonable, whilst for the higher pressure the agreement becomes worse. The excellent agreement between the measurements and the calculation based on [33] is remarkable, especially for void fractions $\epsilon > 0.6$. This would impose the use of [33] for calculating the two-phase sonic velocity, instead of [26]. However, intention of the presented paper is not the derivation of a new relationship for the two-phase sonic velocity, but the calculation of the discharge characteristics of orifices. This requires a suitable relationship for the effective two-phase flow velocity for which Nguyen derived [5]. Furthermore, for choked flow conditions, Nguyen found the effective flow velocity u_{eq} to be identical with the sonic velocity a_{hom} calculated by [26] and obtained excellent agreement with experimental data. For this reason, Nguygen's relationship for the sonic velocity is used here to calculate the critical effective flow velocity. The influence of the two-phase sonic velocity and the equivalent density on the calculated critical mass flow rate is illustrated below in figure 6.

3. COMPUTATIONAL PROCEDURE

The purpose of the proposed procedure is to compute mass flow rate–pressure drop characteristics for constant mass flow qualities in the range $0.1 \leqslant \dot{x} \leqslant 1.0$. The calculation of the complete set of characteristics is started with pure air flow ($\dot{x} = 1.0$) and continued with the successive calculation of characteristics for decreasing mass flow quality. The calculation of each characteristic for a constant mass flow quality $\dot{x}$ is started with the choked flow condition, where critical mass flow rate and critical pressure ratio have to be calculated. For the calculation of the subsequent subcritical flow conditions, for specified mass flow rates the associated pressure ratios have to be calculated. The solving procedure for choked flow conditions with $\dot{x} < 1.0$ is schematically shown in figure 4. Independent variables are the orifice geometry d and D, the total mass flow quality $\dot{x}$ and p_1 and T_1 describing the inlet condition. In order to reduce computation time, the available solution for the critical condition of the preceding characteristic is used to take initial values for the following dependent variables $A_{core,1}$, $A_{core,3}$, $u_{film,1}$, $u_{film,3}$, $\dot{x}_{core}$, EF, n, $\dot{M}_{total}$ and the ratio of the droplet velocities $u_{fac} = u_{drop,3}/u_{drop,1}$. In a first step, the mist core flow is considered to calculate $\rho_{G,3}$, $T_{G,3}$, s_3, ϵ_3, $u_{G,3}$, $u_{G,1}$, $u_{drop,3}$, the critical pressure ratio p_3/p_1 and furthermore new values for the polytropic coefficient n and the droplet velocity ratio u_{fac}, keeping the other predefined dependent variables constant. Because of the complexity the equations used are solved iteratively by using a routine for finding zero values of a function. The function to be solved is a complex combination of [2], [3], [5], [6], [7], [10], [12], [13], [14], [26] and [32] with two internal iterations. After the zero value of the function is found, values for $\rho_{G,3}$, $T_{G,3}$, s_3, ϵ_3, $u_{G,3}$, $u_{G,1}$, u_{fac}, n and p_3/p_1 are obtained, which however, correspond with the initial values for the other predefined dependent variables. Therefore, in a next step new values for EF, $\dot{x}_{core}$, $A_{core,1}$, $u_{film,1}$ and $\dot{M}_{total}$ are calculated by [18], [21], [16], [3] and [1], respectively, and the preceding calculation is repeated with

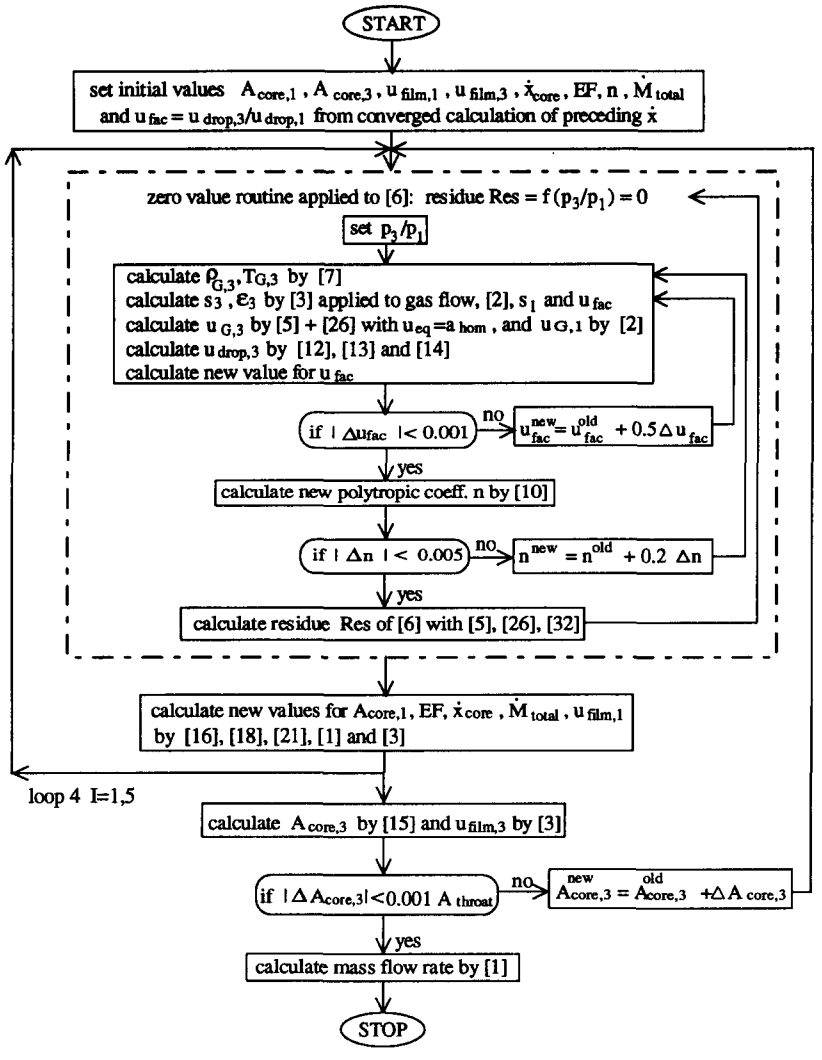

Figure 4. Flow chart of the calculation procedure for the critical flow condition.

these new values. For this loop the number of iterations is set to a value of 5 which is sufficient to obtain convergence for all five variables, and still corresponds with the initial values for $A_{core,3}$ and $u_{film,3}$. Then, by the use of [15] and [3], new values for $A_{core,3}$ and $u_{film,3}$ are calculated based on the other dependent variables. Consequently, the complete procedure is repeated until convergence for $A_{core,3}$ is obtained and the final critical mass flow rate is calculated by [1] applied to the throat cross-section.

The solving procedure for subcritical flow conditions in principle is similar to that for choked flow conditions, however, less complicated. Because the total mass flow rate $\dot{M}_{total}$ is specified and only the associated pressure ratio has to be calculated, the values for $A_{core,1}$, $u_{film,1}$, $\dot{x}_{core}$ and EF may be calculated in a straightforward manner. The remaining dependent variables for which initial values are taken from the preceding calculated flow condition of the same characteristic are $A_{core,3}$, $u_{film,3}$, n and u_{fac}. A difference compared with figure 4 exists for the calculation of the effective two-phase velocity u_{eq} at the throat cross-section 3. Whilst for critical flow conditions u_{eq} is calculated by [26], setting $u_{eq} = a_{hom}$, for subcritical flow conditions u_{eq} is calculated by a rearranged form of [1]. Substituting u_G and u_{drop} by the slip ratio s and the definition for u_{eq}, given by [5], [1] may be rewritten as $u_{eq} = \dot{M}_{core}/\{[(1-\epsilon)s + \epsilon][\epsilon\rho_G + (1-\epsilon)\rho_L/s]\}$. Another difference compared with figure 4 is the omission of loop 4 and the preceding block for calculating new values for $A_{core,1}$, EF, $\dot{x}_{core}$, $\dot{M}_{total}$ and $u_{film,1}$ and the omission of the last block for calculating the mass flow rate.

4. RESULTS AND DISCUSSION

For assessment and verification, the proposed method is compared with other methods known from the literature and with experimental data. Due to the lack of air–oil data in the literature, comparisons were also made with results from air–water investigations.

Figure 5 shows the critical pressure ratio (static pressures) of a mist flow through an orifice (no liquid film) against core mass flow quality for various effective orifice diameters. (The predictions here were obtained using a simplified version of the program outlined in figure 4, since both $A_{core,1}$ and $A_{core,3}$ are known and $\dot{x} = \dot{x}_{core}$). As can be seen, a family of curves is obtained with a maximum critical pressure ratio occurring at approximately $\dot{x}_{core} \approx 0.2$ for all diameter ratios. Moreover, increasing the diameter ratio increases the critical pressure ratio. For pure air flow ($\dot{x}_{core} = 1.0$) this increase agrees with basic gas dynamic equations. It should be noted that reducing the diameter ratio below 0.5 does not decrease the critical pressure ratio below that shown for $d_{eff}/D = 0.5$. The maximum values of the critical pressure ratio correspond to $d_{eff}/D = 1.0$, in which case the ratio is $p_3/p_1 = 1.0$, representing a frictionless pipe flow ($C_D = 1.0$). Starting with pure air the curves for smaller diameter ratios show a significant increase of the critical pressure ratios with decreasing mass flow qualities (increasing oil share). This has to be seen in line with the sharp decrease of the two-phase sonic velocity with increasing oil share, shown in figure 3. The curves for greater diameter ratios show first a slight decrease of the critical pressure ratios with decreasing mass flow qualities, followed by a significant increase of the critical pressure ratios. Unfortunately, no experimental measurements are available for comparison with predictions. However, for the annular–mist flow pattern considered in the present work, the core mass flow quality is normally in the range $\dot{x}_{core} \geqslant 0.75$, i.e. the calculated critical pressure ratios are very close to the values for pure air flows, and it is believed therefore, that any inaccuracies in the calculation of the critical pressure ratio for the present application are small and acceptable.

Figure 6 shows a comparison between the present method, the method of McNeil & Morris (1988), the well-known homogeneous equilibrium model and a simplified version of the proposed method using the frozen sonic speed and the classic mean density (see Wallis 1969) instead of [26] and [32], respectively. Furthermore, the methods are compared with air–water measurements of Chen *et al.* for critical flow conditions. Plotted is the total mass flow rate versus the total mass flow quality. For lower mass flow qualities, the homogeneous model neglecting phase slip and flow pattern and the simplified model show appreciable deviations from the experimental data. The difference between both methods is mainly a result of the entrainment effect, which is neglected in the homogeneous model. The comparison between the simplified model and the proposed method illustrates the combined influence of different two-phase sonic velocities and different equivalent densities on the calculated critical mass flow rate. With decreasing two-phase sonic

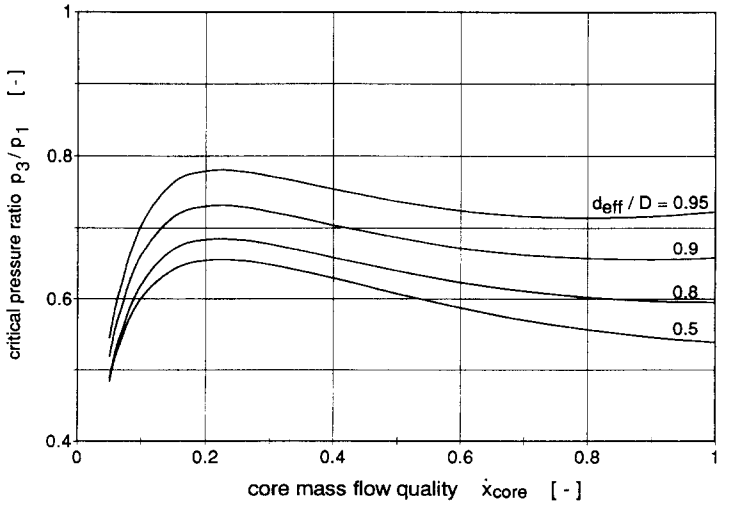

Figure 5. Critical pressure ratio across an orifice for air–water mist flow at $p_1 = 2.0$ bar and $T_1 = 373$ K.

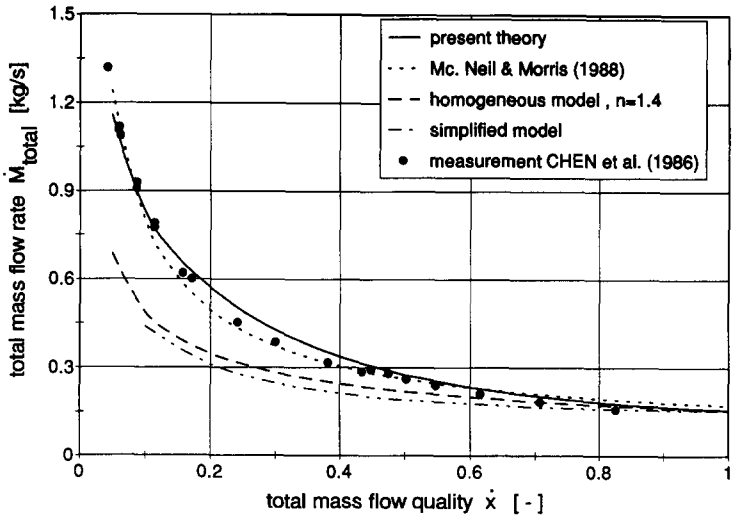

Figure 6. Critical total mass flow rate—comparison of calculation and measurement for an orifice with $D = 50.8$ mm and $d = 22.4$ mm at $p_1 = 1.98$ bar and $T_1 = 293$ K.

velocity the core flow cross-section area A_{core}, the film velocity u_{film}, the gas velocity and consequently the droplet velocity decrease, whilst the core void fraction and the film flow cross-section area A_{film} increase. The total effect of a lower two-phase sonic velocity (as in the simplified model) is an appreciable reduction in the critcal mass flow rate. Between the method of McNeil & Morris, the proposed method and the experimental data there is a very good agreement across the complete range of mass flow qualities. Both methods likewise are shown to be able to predict the measurements.

In figures 7 and 8 the proposed method is compared with the experimental results for air–oil mixtures from Wood & Dickson for critical flow conditions. Because the inlet pressure p_1 was not kept constant in the experiments but varied between $p_1 = 1.81$ bar and $p_1 = 4.81$ bar, in order to keep the number of graphs to a minimum, it was decided to plot the relative deviation between calculation and experiment first against the total mass flow quality and second against the inlet pressure. Whilst for $T_1 = 295$ K the agreement between calculation and experiment is fairly good,

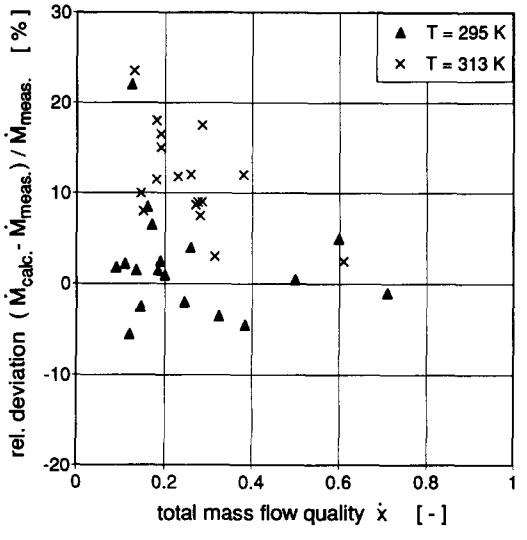

Figure 7. Relative deviation between predicted and measured mass flow rates for critical air–oil flows through an orifice with $D = 37.9$ mm and $d = 9.55$ mm.

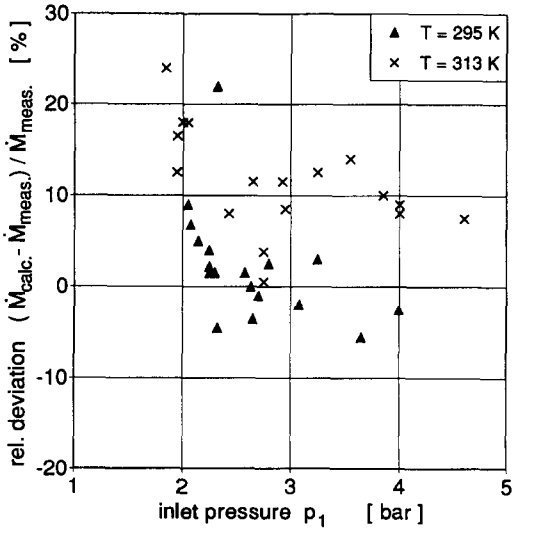

Figure 8. Relative deviation between predicted and measured mass flow rates for critical air–oil flows through an orifice with $D = 37.9$ mm and $d = 9.55$ mm.

for $T_1 = 313$ K the average deviation is about 12%. For this phenomenon of temperature dependence, no explanation can be given. Moreover, for both inlet temperatures, the deviation tends to increase at lower inlet pressure. Considering figures 6, 7 and 8, the proposed method is shown to be able to predict experimental data for critical gas–liquid flows through orifices with reasonable accuracy. A comparison between the method of McNeil & Morris and the air–oil data analogous to figures 7 and 8 is not presented. Because both methods produce comparable results, the obtained scatter bands for the relative deviations are similar to figures 7 and 8.

Figure 9 shows the influence of phase slip and entrainment fraction on the critical total mass flow rate in dependence of the orifice diameter ratio d/D. Compared are the calculated mass flow rates obtained by the basic configuration of the proposed method and mass flow rates obtained by simplified versions with the phase slip and/or the entrainment fraction EF set to unity. The consequence of an increased entrainment fraction is a decrease of core mass flow quality and core void fraction and a decrease of the critical flow velocity. The effect of a phase slip ratio of $s = 1.0$ is opposite and results in an increase of core void fraction and critical flow velocity. As can be seen, the calculation for full entrainment (EF = 1.0) differs from the basic calculation only slightly (underprediction up to 14%) for smaller diameter ratios, where the calculated entrainment fraction in the basic calculation is below unity. With increasing diameter ratio, the flow velocity upstream of the orifice increases and the entrainment fraction in the basic calculation approaches to unity. For subcritical flow conditions, where the flow velocity depending on the pressure ratio is lower, the difference between the basic calculation and the calculation for full entrainment is more distinct. The calculation for $s = 1.0$ shows another behaviour. For small diameter ratios, the modified calculation agrees with the basic calculation. Because of the lower entrainment fraction the phase slip in the core flow is of minor influence. With increasing diameter ratio, the entrainment fraction, i.e. droplet load increases and the effect of $s = 1.0$ leads to increased critical mass flow rates (overprediction up to 40%). The calculation for EF = 1.0 and $s = 1.0$ shows for greater diameter ratios the expected behaviour; the calculation agrees with the calculation for $s = 1.0$. For lower diameter ratios the calculated mass flow rates are higher than those obtained by the basic calculation and the calculation for $s = 1.0$. The effect of $s = 1.0$ leading to higher mass flow rates is intensified by the increased entrainment fraction (EF = 1.0). Considering the effects obtained, the phenomena of phase slip and entrainment are not negligible.

Figure 10 shows a comparison between the widely used method of Simpson (1983) with application to incompressible flows, the proposed method, the method of Morris (1991) for subcritical flows and the well-known homogeneous equilibrium model. Each method is used to calculate the pressure ratio across a specified orifice for an air–water flow with a specified constant mass flow rate and variable mass flow quality. As can be seen, the homogeneous model and the

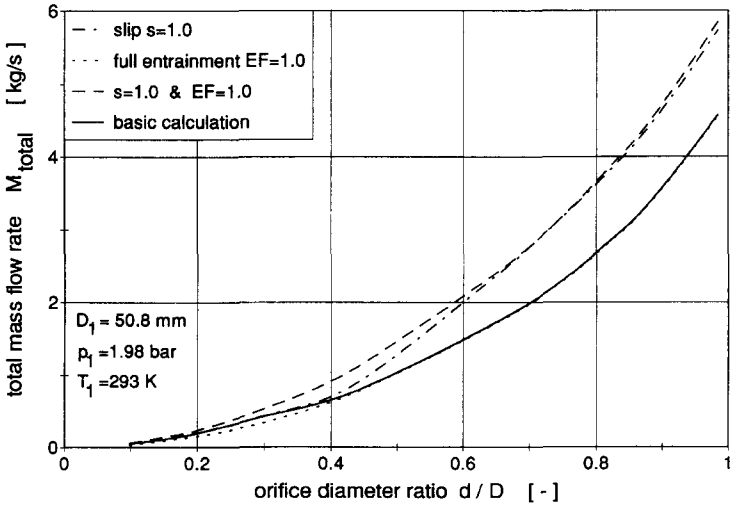

Figure 9. Influence of phase velocity and entrainment fraction on the critical mass flow rate at a mass flow quality of $\dot{x} = 0.1$.

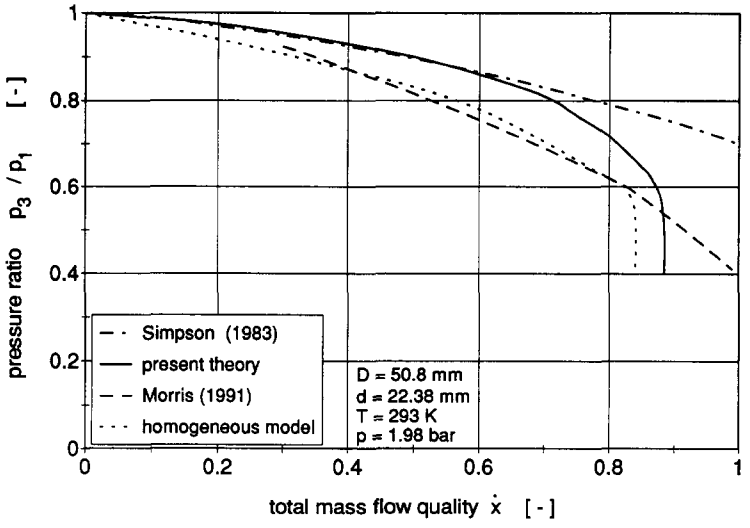

Figure 10. Comparison of calculated pressure ratios across an orifice for air–water flows with a constant mass flow rate of $\dot{M} = 0.17$ kg/s.

proposed method show a similar trend. With increasing mass flow quality, the pressure ratio across the orifice decreases until the critical flow condition is reached at mass flow qualities of $\dot{x} = 0.83$ and $\dot{x} = 0.885$, respectively (characteristics become vertical). According to these methods, for higher mass flow qualities the specified mass flow rate cannot be discharged any more through the specified orifice. The methods of Simpson and Morris show a decreasing pressure ratio with increasing mass flow quality across the complete range of $\dot{x}$. Whilst Simpson does not reach the choked flow condition (pressure ratios higher than 0.7), Morris produces results clearly beyond the critical flow condition. Therefore, a reasonable application of the method of Morris requires additional information about the limiting critical pressure ratio. The method of Simpson is derived for incompressible flows and it is expected therefore, to predict unrealistic values for high mass flow qualities, where the amount of air and consequently the air velocity is high due to the constant mass flow rate and compressibility effects occur. Noteworthy is the good agreement between the homogeneous model and the method of Morris for mass flow qualities $\dot{x} \leqslant 0.8$ and the good agreement between the proposed method and the Simpson method for mass flow qualities $\dot{x} \leqslant 0.6$.

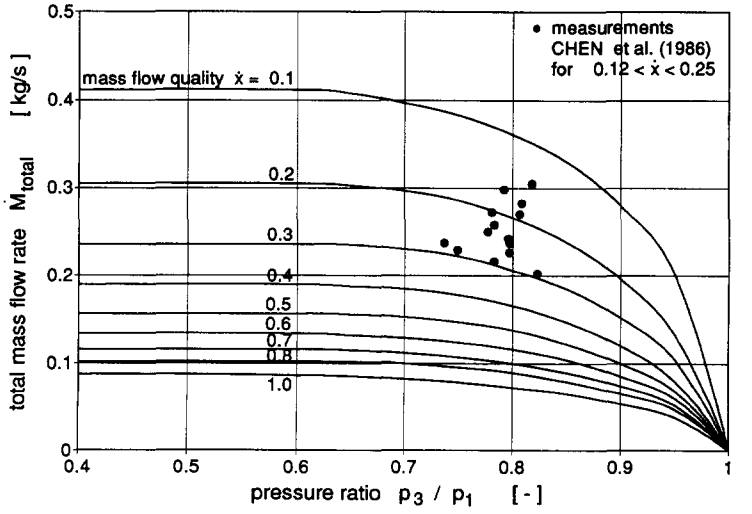

Figure 11. Discharge characteristic of an orifice with $D = 25.4$ mm and $d = 13.7$ mm for air–water flow at $p_1 = 2.96$ bar and $T_1 = 293$ K.

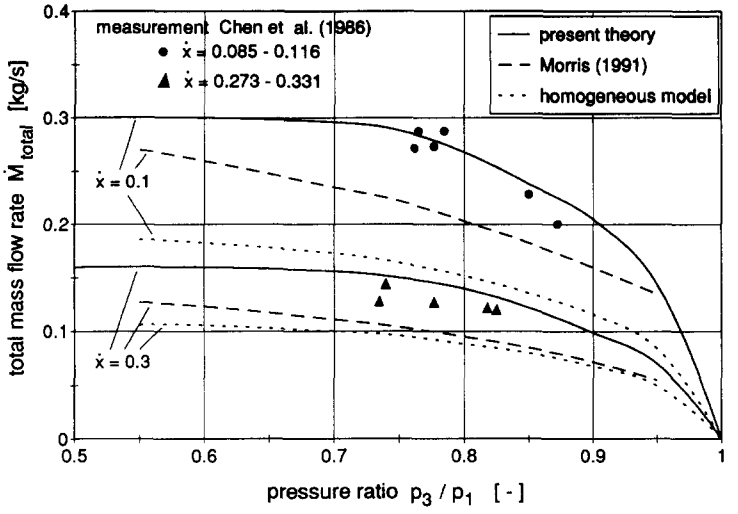

Figure 12. Comparison of calculated mass flow rates with measurements for air–water flows at $p_1 = 1.98$ bar and $T_1 = 293$ K for an orifice with $D = 25.4$ mm and $d = 13.7$ mm.

In figure 11, a complete set of discharge characteristics calculated by the proposed method for a typical geometry and inlet condition is shown and compared with some air–water measurements with total mass flow qualities in the range $0.12 \leqslant \dot{x} \leqslant 0.25$. The total mass flow rate is plotted versus the pressure ratio across the orifice. The horizontal parts of the characteristics represent choked flow conditions and show a significant increase of the total mass flow rates with decreasing mass flow qualities, which is in agreement with figure 6. The parabolic parts of the characteristics represent subcritical flow conditions and show an expected trend analogous to the well-known characteristic for pure air flow ($\dot{x} = 1$).

Figure 12 shows a comparison between the proposed method, the method of Morris, the homogeneous equilibrium model and air–water measurements of Chen *et al.* for the total mass flow rate plotted versus the pressure ratio across the orifice. For simplification, only two mass flow qualities are considered. The experimental data show a narrow scatter band in the mass flow quality around the nominal values of 0.1 and 0.3, respectively. As can be seen, the proposed method is

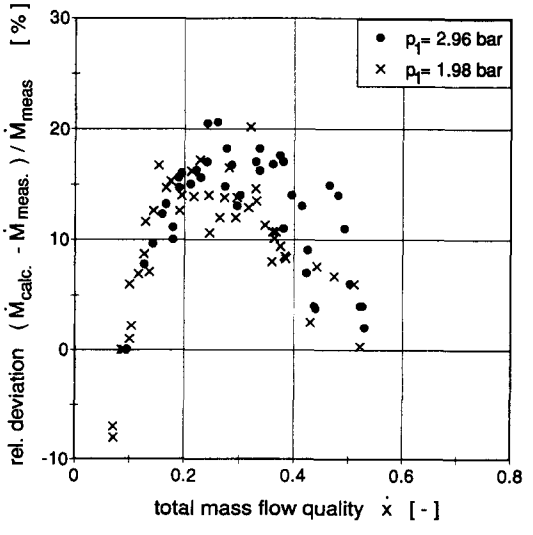

Figure 13. Relative deviation between predicted and measured mass flow rates for air–water flows through an orifice with $D = 25.4$ mm and $d = 13.7$ mm.

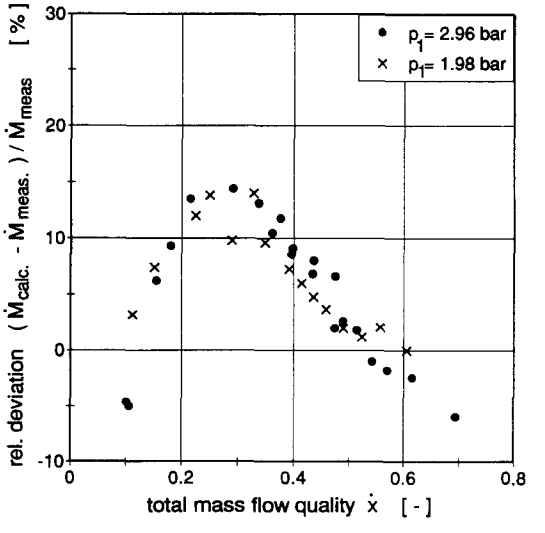

Figure 14. Relative deviation between predicted and measured mass flow rates for air–water flows through an orifice with $D = 25.4$ mm and $d = 15.85$ mm.

in good agreement with the measurements, showing a slight overprediction, whilst Morris and the homogeneous model clearly underpredict the measurements. Furthermore, the method of Morris fails to produce a near horizontal tangent line for flow conditions close to the critical flow condition. Due to the fact that the mass flow quality was not kept constant in the experiments, the available test results cannot easily be compared with the predictions. Therefore, figures 13 and 14 show the relative deviation between calculated and measured total mass flow rate against the total mass flow quality for three orifice geometries and two inlet pressures.

Figures 13 and 14, which are for similar orifices, show the tendency of a maximum deviation to occur at total mass flow qualities in the range $0.2 \leqslant \dot{x} \leqslant 0.3$. As can be seen from the figures, the results indicate a certain degree of independence with the inlet pressure. However, it should be borne in mind that only two inlet pressures were considered. The variation in the pressure ratio between 0.62 and 0.91 was achieved by altering the exit pressure. A dependence of the relative deviation with the pressure ratio cannot be identified. A comparison between the method of Morris and the experimetnal data analogous to figure 13 shows relative deviations between -15 and -23% for $p_1 = 2.96$ bar (average deviation -20%) and relative deviations between -18 and -25% for $p_1 = 1.98$ bar (average deviation -22%).

Compared with figure 13, the deviations obtained are appreciably higher, but in contrast to figure 13, for both pressures, a nearly homogeneous distribution for the relative deviations across the mass flow quality, without maximum, is obtained. This indicates a weakness of the proposed method for subcritical flow conditions with mass flow qualities in the range $0.2 \leqslant \dot{x} \leqslant 0.3$.

5. CONCLUSIONS

A new method is proposed for calculating pressure drop discharge characteristics of annular–mist two-component gas–liquid flows through orifices under aero-engine conditions (low pressures). This includes subcritical and choked flow conditions. The method is based upon a flow model, which takes account of the basic flow phenomena of the flow pattern considered. The method differs between the annular liquid film flow and the mist core flow, which determines the pressure drop across the orifice. The assumed vena contracta effect of the mist core flow is approximately accounted for by applying discharge coefficients for pure air flows. The phase slip ratio of the mist core flow at the orifice throat cross-section is calculated under consideration of the orifice geometry and the pressure ratio across the orifice by a force balance model applied to spherical droplets. Based on a relationship for calculating the sonic velocity in a homogeneously distributed gas–liquid flow, a new equivalent two-phase density has been derived, which characterizes the compressibility of a homogeneously distributed gas–liquid fluid.

For assessment and verification, the proposed method is compared with the well-known homogeneous equilibrium model, the method of Simpson for incompressible flows, the method of Morris for subcritical flows, the method of McNeil & Morris for critical flows and with the available air–water and air–oil measurements for different orifices and different inlet conditions. For critical flow conditons the proposed method and likewise the method of McNeil & Morris show to be able to predict the experimental data with good accuracy for two-phase flows. For subcritical flow conditions, the proposed method tends to overpredict the measurements, especially for mass flow qualities in the range $0.1 \leqslant \dot{x} \leqslant 0.5$. However, compared with the other methods investigated, which show distinct underpredictions of the measurements, the proposed method shows unambiguously the best agreement with the experimental data. Furthermore, the proposed method covers the complete range of flow conditions from incompressible to choked flows. A change between different methods, which are applicable only to incompressible, subcritical or choked flow conditions, is not necessary and the problem of determining transition regions between different methods is avoided.

The computation time on a mainframe computer for a complete set of characteristics is in the range of seconds. Therefore, the proposed method represents a useful, quick, cheap and reliable design tool for practical engineering. Further testing of the method is necessary, but this requires additional experimental data for air–oil mixtures.

REFERENCES

Andreussi, P., Romano, G. & Zanelli, S. 1978 Droplet size distribution in annular–mist flows. *Ist International Conference on Liquid Atomization and Spray Systems*, Tokyo, Japan, 27–31 August 1978.

Azzopardi, B. J., Piearcey, A. & Jepson, D. M. 1991 Drop size measurements for annular two-phase flow in a 20 mm diameter vertical tube. *Exp. Fluids* **11,** 191–197.

Bragg, S. L. 1960 Effect of compressibility on the discharge coefficient of orifices and nozzles. *J. Mech. Engng Sci.* **2,** 35–44.

Chen, D. K., Chen, Z. H., Zhao, Z. S. & Zhuo, N. 1986 The local resistance of gas–liquid two-phase flow through an orifice. *Int. J. Heat Fluid Flow* **7,** 231–238.

Chisholm, D. 1983 *Two-phase Flow in Pipelines and Heat Exchangers*. Goldwin, London.

Idel'chik, I. E. 1986 *Handbook of Hydraulic Resistance*, 2nd edn. Hemisphere, Washington, DC.

Ishii, M. & Mishima, K. 1989 Droplet entrainment correlation in annular two-phase flow. *Int. J. Heat Mass Transfer* **32,** 1835–1846.

Kataoka, I., Ishii, M. & Mishima, K. 1983 Generation and size distribution of droplet in annular two-phase flow. Presented at *ASME Applied Mechanics, Bioengineering and Fluids Engineering Conference*, Houston, TX, 20–22 June 1983, Paper No. 83-FE-2.

Kulov, N. N., Maksimov, V. V., Maljusov, V. A. & Zhavoronkov, N. H. 1979 Pressure drop, mean film thickness and entrainment in downward two-phase flow. *Chem. Engng J.* **18,** 183–188.

Kutz, K. J. & Speer, T. M. 1992 Simulation of the secondary air system of aero-engines. Presented at *ASME Int. Gas Turbine and Aeroengine Congress and Exposition*, Cologne, Germany, 1–4 June 1992, Paper No. 91-GT-68.

McNeil, D. A. & Morris, S. D. 1988 *Proceedings of 2nd National Heat Transfer Conference*, Glasgow, U.K., Vol. 2, pp. 1243–1256.

Morris, S. D. 1990 Discharge coefficients for choked gas-liquid flow through nozzles and orifices and applications to safety devices. *J. Loss Prev. Process Ind.* **3,** 303–310.

Morris, S. D. 1991 Compressible gas–liquid flow through pipeline restrictions. *Chem. Engng Process.* **30,** 39–44.

Nguyen, L. D. 1981 Schallgeschwindigkeit und kritischer Massendurchsatz in Ein- und Zweikomponentigen Gas–Flüssigkeitsströmungen. Dissertation, Lehrstuhl C für Thermodynamik, Technische Universität München.

Pilch, M. & Erdman, C. A. 1987 Use of breakup time data and velocity history data to predict the maximum size of stable fragments for acceleration-induced breakup of liquid drops. *Int. J. Multiphase Flow* **13,** 741–757.

Prandtl, L., Oswatitsch, L. & Wieghart, K. 1984 *Führer durch die Strömungslehre*. Vieweg, Braunschweig.

Semenov, N. I. & Kosterin, S. I. 1967 Acoustic velocity in two-phase flow. *Symposium on Two-phase Flow Dynamics*, A 68–11153.

Simpson, H. C. 1983 Two-phase flow through gate valves and orifice plates. *BHRA Fluid Engineering*, pp. 28–32.

Wallis, G. B. 1969 *One-dimensional Two-phase Flow*. McGraw–Hill, New York.

Wood, J. D. & Dickson, A. N. 1973 Metering of air–oil mixtures with sharp-edged orifices. Dep. Mech. Eng. Rep., Heriot-Watt University, Riccarton, Edinburgh, U.K.

Zimmermann, H., Kammerer, A., Fischer, R. & Rebhan, D. 1991 Two-phase flow correlations in air/oil systems of aero-engines. Presented at *ASME Int. Gas Turbine and Aeroengine Congress and Exposition*, Orlando, FL., 3–6 June 1991, Paper No. 91-GT-54.

APPENDIX A

Notes on the Derivation of [15]

With the assumption that the liquid film enters the control volume without having momentum in the z-direction, the application of the momentum equation to the control volume shown in figure 1 has the form

$$\rho_{G,2}A_{eff}\epsilon_2 u_{G,2}^2 + \rho_L A_{eff}(1-\epsilon_2)u_{drop,2}^2 - \rho_{G,3}A_{core,3}\epsilon_3 u_{G,3}^2 - \rho_L A_{core,3}(1-\epsilon_3)u_{drop,3}^2 - \rho_L(A_{eff} - A_{core,3})u_{film,3}^2 = A_{eff}(p_3 - p_2). \quad [A1]$$

Introducing the continuity equations for the gaseous phase of the core flow and the liquid film flow and furthermore using the correlation for the entrainment fraction of section 2.3, the liquid film velocity at section 3 may be written as:

$$u_{film,3} = \frac{(1-\dot{x})}{\dot{x}} \frac{\rho_{G,1}A_{core,1}\epsilon_1 u_{G,1}}{\rho_L(A_{eff} - A_{core,3})}(1 - EF). \quad [A2]$$

Substituting [A2] in [A1], after some algebra, [A1] may be rewritten as:

$$(A_{eff} - A_{core,3})^2 + \frac{C_1}{C_2}(A_{eff} - A_{core,3}) - \frac{C_3}{C_2} = 0, \quad [A3]$$

with

$$C_1 = \rho_{G,2}A_{eff}\epsilon_2 u_{G,2}^2 + \rho_L A_{eff}(1-\epsilon_2)u_{drop,2}^2 - \rho_{G,3}A_{eff}\epsilon_3 u_{G,3}^2 - \rho_L A_{eff}(1-\epsilon_3)u_{drop,3}^2 - A_{eff}(p_3 - p_2), \quad [A4]$$

$$C_2 = \rho_{G,3}\epsilon_3 u_{G,3}^2 + \rho_L(1-\epsilon_3)u_{drop,3}^2, \quad [A5]$$

$$C_3 = (1-EF)^2\left(\frac{1-\dot{x}}{\dot{x}}\right)^2 \frac{(\rho_{G,1}A_{core,1}\epsilon_1 u_{G,1})^2}{\rho_L}. \quad [A6]$$

Because the change in the core flow cross-section between sections 2 and 3 is small compared with the change between sections 1 and 3, and furthermore, sections 2 and 3 are relatively close to each other, to a good approximation for practical application, the droplet velocity u_{drop} and the core void fraction ϵ can be kept constant between sections 2 and 3, i.e. $u_{drop,3} \approx u_{drop,2}$ and $\epsilon_2 \approx \epsilon_3$.

In addition, the flow of the gaseous phase between sections 2 and 3 can be assumed to be adiabatic and in the first approximation frictionless. Consequently, basic gas dynamic equations may be applied to the gaseous phase of the mist core flow to express the flow condition at section 2 by values of the flow condition at section 3. Introducing the definition of the flow function

$$\psi = \frac{A^*}{A} = \left(\frac{\kappa+1}{2} - \frac{\kappa-1}{2}M^{*2}\right)^{1/(\kappa-1)} M^*, \quad [A7]$$

where κ is the isentropic coefficient, M^* is the critcal Mach number, A is the flow cross-section, A^* is the flow cross-section at sonic condition and furthermore setting

$$A_3^* \approx A_2^*, \quad [A8]$$

the flow function at section 2 may be expressed as:

$$\psi_2 \approx \psi_3 \frac{A_{core,3}}{A_{eff}}. \quad [A9]$$

Applying [A7] to section 2 and substituting [A9] in [A7] an equation is obtained, which can be solved for the critical Mach number at section 2, M_2^*. Consequently, the unknown values at section 2 may be expressed in the form

$$u_{G,2} = M_2^*\sqrt{\frac{2\kappa}{\kappa+1}\left(T_3 + \frac{u_{G,3}^2}{2c_{pL}}\right)} \quad [A10]$$

$$\rho_{G,2} = \rho_{G,3}\left[\frac{1 - \frac{\kappa-1}{\kappa+1}M_2^*}{1 - \frac{\kappa-1}{\kappa+1}M_3^*}\right]^{1/(\kappa-1)} \quad [A11]$$

$$p_2 = p_3\left[\frac{\rho_{G,2}}{\rho_{G,3}}\right]^{\kappa}, \quad [A12]$$

and C_1 reduces to a function, which depends only on values of the flow condition at section 3.